Clays and Clay Minerals, Vol. 41, No. 1, 45–55, 1993.

QUANTITATIVE ANALYSIS OF MIXTURES OF 1*M* AND 2M_1 DIOCTAHEDRAL MICAS BY X-RAY DIFFRACTION

RODNEY T. TETTENHORST AND CHARLES E. CORBATÓ

Department of Geological Sciences, The Ohio State University
Columbus, Ohio 43210

Abstract—Investigation of a naturally occurring mixture of dioctahedral micas prompted an examination of X-ray diffraction (XRD) techniques for obtaining quantitative estimates of 1*M* and 2M_1 mica proportions. A method for determining quantitative estimates has been developed that includes the effect of preferred orientation of mica particles as described by the March function. A diagram is presented from which the percentage of 2M_1 and the March parameter (r) can be obtained from two peak-area ratios: 2.80 Å/5.0 Å and 2.80 Å/2.58 Å, which are measured on observed XRD patterns of mica mixtures. The ability of this peak-area ratio diagram to predict reasonably accurate proportions of 1*M* and 2M_1 micas was tested by comparing calculated and observed XRD patterns over a range of 2θ values from 16° to 40° for size-fractionated mixtures. Lack of accurate crystal-structure data for dioctahedral 1*M* mica proved an impediment to obtaining improved quantitative estimates of mica proportions.

Key Words—March function, Peak-area ratio, Preferred orientation, Quantitative analysis, X-ray diffraction, 1*M* mica, 2M_1 mica.

INTRODUCTION

Coexisting 1*M* and 2M_1 dioctahedral micas are common in the geologic record and occur in or are formed from a variety of rock types: limestone (Reynolds, 1963), argillite or shale (Maxwell and Hower, 1967; Foscolos and Kodama, 1974), bentonite (Środoń and Eberl, 1984), volcanic glass (Inoue *et al.*, 1987), volcanic flows and tuff (Eberl *et al.*, 1987), and a pegmatite dike (Foord *et al.*, 1991). Frequently, the proportion of the two micas is estimated by X-ray diffraction (XRD) to aid in understanding the evolution or history of a suite of rocks. Explanations of variations in the proportions of 1*M* and 2M_1 micas often are based on the laboratory studies of Yoder and Eugster (1955), who found that 2M_1 mica is stable at elevated temperatures, and Velde (1965), whose data indicated that 2M_1 mica having the ideal muscovite chemical composition is the only stable form. An increase in the relative amount of 2M_1 mica has been correlated with an increase in temperature and pressure accompanying deep burial (Maxwell and Hower, 1967), grade of metamorphism (Weaver and Broekstra, 1984), and intensity of hydrothermal alteration (DiMarco *et al.*, 1989). Velde and Hower (1963) found a greater proportion of 2M_1 mica with increasing grain size in shales; and Eberl *et al.* (1987) found that the proportion of the two micas is independent of particle size in sericites. Because a reliable estimate of the proportion of the two micas may be important in assessing the role of geologic parameters that influence rock history, a reconsideration of XRD techniques used to estimate quantities seems appropriate.

XRD procedures for estimating proportions of 1*M* and 2M_1 micas in mixtures developed by Reynolds (1963), Velde and Hower (1963), and Maxwell and Hower (1967) have been used extensively (Kisch, 1983). Each method involves measuring the area of a peak unique to 2M_1 mica and dividing it by the area of a peak common to both micas. Reynolds (1963) used the 3.00 Å peak; Velde and Hower (1963) used the 3.74 Å peak; and Maxwell and Hower (1967) used the 2.80 Å peak for the unique 2M_1 peak. These investigators employed the 2.58 Å peak, which is common to both micas, and in each case a curve relating the percentage of 2M_1 mica in a mixture to a peak-area ratio was obtained from experimental measurements. Reynolds (1963) and Maxwell and Hower (1967) determined the appropriate peak-area ratio from a ground muscovite and assumed a linear relationship for the % 2M_1 in mixtures of the two micas. Velde and Hower (1963) mixed a 2M_1 mica with a 1*M* mica in several proportions and obtained non-linear relationships for two size fractions (<1 μm and >1 μm). The procedure of Maxwell and Hower (1967) often is preferred because, although the 2.80 Å peak of 2M_1 mica is relatively weak, it is free of interference from common non-clay impurities such as feldspar and calcite.

These methods allow proportions of 1*M* and 2M_1 micas to be obtained with relative ease, which is advantageous in studies involving numerous samples. A disadvantage of these methods is that the obtained proportions of 1*M* and 2M_1 micas are not accurate although they may allow a suite of samples from a given geologic setting to be arranged relative to 1*M*–2M_1 content. X-ray techniques involving Rietveld refinement or whole-pattern fitting *may* be capable of

providing more exact quantities, but most investigators cannot devote the time or resources to perform such analyses on a suite of samples.

A tacit assumption of X-ray techniques described in past studies is that orientation of mica particles is constant in all sample mounts and comparable to that in the standards. This situation is unlikely even though care may be taken to prepare all specimens used for XRD in the same way. In addition, several *hkl* planes contribute to the intensity of a peak that is used for quantitative estimates of the two micas. These *hkl* planes make various angles with the plane of preferred orientation (001 for micas) and contribute an intensity that depends in part on the degree of preferred orientation in sample mounts. Consequently, quantitative estimates of proportions of $1M$ and $2M_1$ micas from previous studies that neglected the effect of orientation may be inexact.

Dollase (1986) proposed that preferred orientation be described by a function originally proposed by March (1932) for rock deformation. To our knowledge, no systematic study of the utility of this function to account for preferred orientation of mica particles in specimens prepared for XRD has been presented although it has been incorporated into refinement programs (e.g., Post and Bish, 1989). The March function is $(r^2\cos^2\xi + r^{-1}\sin^2\xi)^{-3/2}$, where ξ is the angle between an *hkl* plane and the preferred orientation plane, and r is the single variable that is a measure of orientation. An r equal to unity represents an unoriented, "random" condition; for planar particles, $r < 1.0$ describes a preferred orientation often generated by the common methods of preparing samples, which produce a flat surface for presentation to the X-ray beam. Improved accuracy of proportions of $1M$ and $2M_1$ micas may result if particle orientation is taken into account, assuming the March function provides an adequate description of particle orientation in two-mica specimens prepared for XRD.

The main goal of the present study is to analyze and characterize a two-mica mixture and to develop, based on the work of Maxwell and Hower (1967), a simple method of accurately estimating proportions of $1M$ and $2M_1$ micas that accounts for particle orientation as described by the March function. Our interest in estimating proportions of $1M$ and $2M_1$ micas in mixtures arose during an XRD examination of the natural sample described in this report, which showed the presence of two micas and a range of particle sizes from <2 μm to 4 mm.

MATERIAL

The investigated specimen was collected from an apparent fault zone in a cliff face of Paleozoic rocks on the west coast of Cape Breton Island, Nova Scotia, Canada, on the Gulf of St. Lawrence, approximately 2 km south of a promontory called Cap Rouge. The approximate location of the outcrop is latitude 46°43′N and longitude 60°56′W at the mouth of Trout Brook. When collected, the sample was white, very wet, and plastic. An XRD pattern of a portion of the dried, powdered bulk Cap Rouge sample shows the presence of mica, quartz, and a small amount of jarosite. The material disperses readily in water with hand-stirring and without chemical or other mechanical aids.

Preliminary XRD and chemical analyses revealed two micas, one concentrated in the 0.4–4 mm fraction and the other in the <2 μm fraction. Bargar (1990) examined mica flakes (>420 μm) from this Cap Rouge sample using X-ray precession methods described by Bailey (1988). All flakes examined by Bargar were $2M_1$. An XRD pattern of a relatively unoriented portion of the <2 μm fraction can be indexed as $1M$. Bargar also determined by microprobe the chemical composition of the $2M_1$ and $1M$ micas. The structural formula calculated from the measured chemistry for the $2M_1$ mica (mean of three measurements) is

$$K^{1+}_{0.90}Na^{1+}_{0.10}Ba^{2+}_{0.01} \cdot (Al^{3+}_{1.69}Ti^{4+}_{0.07}Fe^{2+}_{0.09}Mg^{2+}_{0.13})^{VI} \cdot (Si^{4+}_{3.18}Al^{3+}_{0.82})^{IV}O_{10}(OH)_2$$

and for the $1M$ mica (mean of five measurements) is

$$K^{1+}_{0.77}Na^{1+}_{0.02}Ca^{2+}_{0.02} \cdot (Al^{3+}_{1.54}Ti^{4+}_{0.01}Fe^{2+}_{0.15}Mg^{2+}_{0.32})^{VI} \cdot (Si^{4+}_{3.56}Al^{3+}_{0.44})^{IV}O_{10}(OH)_2.$$

Trace amounts of chromium and manganese are present in both samples. A representation of these chemical compositions on a M^+-4Si-R^{2+} diagram (after Meunier and Velde, 1989) is shown in Figure 1. The composition of the $2M_1$ mica falls about midway between the compositions of muscovite and phengite; the composition of the $1M$ mica lies near the line connecting the compositions of 0.75 illite and 0.75 celadonite, about two-thirds of the distance from the 0.75 illite composition.

METHODS OF INVESTIGATION

The focus of the present study was to provide a comparison of observed XRD patterns of the Cap Rouge micas with calculated patterns over the 16° to 40° 2θ range (CuKα), which is definitive and commonly examined for identification of mica types. To do this, several procedures were used.

Size separation

The presence of large $2M_1$ mica flakes (0.4–4 mm) and pure $1M$ mica in the <2 μm fraction of the Cap Rouge specimen suggested that intermediate size fractions might contain mixtures in various proportions. Sizes were separated by wet sieving for >20 μm particles and by settling in water for <20 μm particles.

https://doi.org/10.1346/CCMN.1993.0410105 Published online by Cambridge University Press

Sample preparation for XRD

Coarse size fractions, i.e., >20 μm, were ground by hand, under acetone, and for short times because of deleterious effects observed on XRD patterns of micas with long-term grinding noted in this study and by others (e.g., Yoder and Eugster, 1955). Although some mismatch between calculated and observed XRD patterns may be due to an insufficient number of particles having the correct orientation to diffract X-rays, this is not believed to be a major consideration in this study. No grinding was done on size fractions <20 μm. Most quartz and all detectable jarosite were removed by hand-picking from size fractions >105 μm. Several methods of packing samples for XRD analysis were used, including front-, back-, and side-packing.

Experimental XRD conditions

XRD conditions for most observed patterns were: CuKα (Ni-filter); 35 kV, 15 mA; 0.5° 2θ/min scan speed; 0.25 in/min chart speed; 2 s time constant; and 500 c/s full-scale deflection. Conditions for the pattern of the oriented <2 μm fraction were the same, except for 30 kV, 10 mA, and 1000 c/s full-scale deflection.

Cell parameters

In order to generate calculated patterns, unit cell parameters were obtained from a least-squares analysis of the 2θ values of peaks on XRD patterns taken from relatively unoriented samples of the <2 μm fraction and the 0.4–4 mm fraction. Eight peaks were used for the <2 μm fraction and 14 peaks were used for the 0.4–4 mm fraction. The peaks utilized could be assigned unique *hkl* values.

Calculated patterns

Calculated patterns were obtained from programs of Corbató and Tettenhorst (1982) utilizing the chemical compositions of the micas determined by Bargar (1990). Atomic parameters from Rothbauer (1971) for muscovite (space group C2/*c*) were assumed for the $2M_1$ mica. Rothbauer's atomic parameters were transformed to space group C2/*m* for the 1*M* mica. Neutral-atom scattering factors were used although the effect of ionic scattering factors, including that for O^{2-}, on the calculated patterns was examined. The structure of Sidorenko *et al.* (1975) of 1*M* mica with space group C2 was considered but rejected because of its relatively poor definition.

Determination of March parameters

Heights of selected peaks in the 16° to 40° 2θ range were measured on the calculated and observed XRD patterns of the 1*M* and the $2M_1$ micas. Ten peaks were measured on patterns of the 1*M* mica; 14 peaks were measured on patterns of the $2M_1$ mica. Nearly all peaks had single *hkl* values. Observed and calculated peak heights were then used in a least-squares refinement to yield a value of the March parameter (*r*) and a scale factor for each mica.

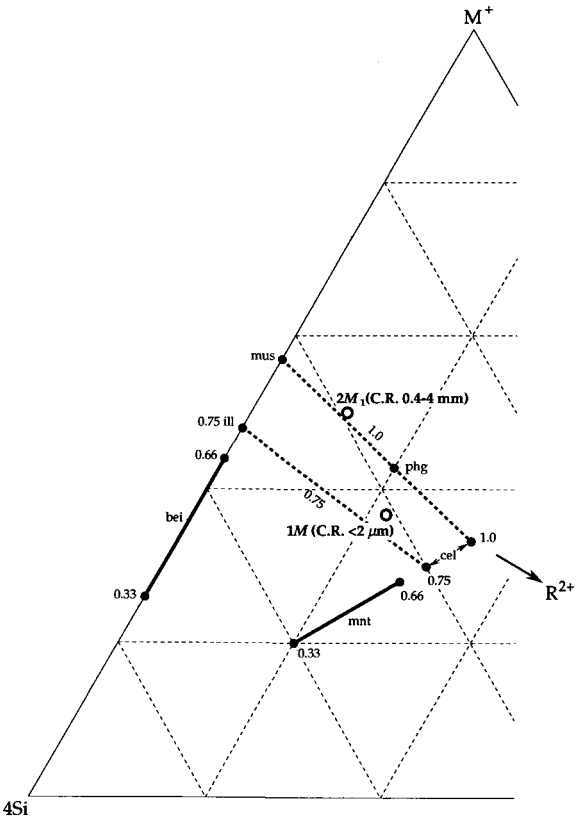

Figure 1. Compositions of Cap Rouge micas (Bargar, 1990; open circles labeled C.R.) compared with various layer silicates (filled circles) on a M^+-4Si-R^{2+} diagram (after Meunier and Velde, 1989). Abbreviations are beidellite (bei), celadonite (cel), illite (ill), montmorillonite (mnt), muscovite (mus), and phengite (phg). Layer charges per $O_{10}(OH)_2$ are given by numbers (0.33, 0.66, 0.75, 1.0). Thick solid lines = accepted compositional ranges. Thick dashed lines = layer charges of 0.75 and 1.0.

RESULTS AND DISCUSSION

General characterization of the two Cap Rouge micas

Unit cell parameters of the two micas were determined in order to produce calculated patterns whose peak positions matched closely those of the observed XRD patterns. Cell parameters of the 1*M* mica were a = 5.220(8) Å, b = 8.983(10) Å, c = 10.176(18) Å, β = 101.15(0)°; those of the $2M_1$ mica were a = 5.205(4) Å, b = 9.021(6) Å, c = 20.078(18) Å, β = 95.67(0)°. Numbers in parentheses represent the standard deviation in the last given significant figure.

Calculated 2θ values and intensities for permissible *hkl* values of the two micas, based on the determined cell parameters, the chemical compositions of Bargar (1990), and the structure and atomic parameters of Rothbauer (1971), are given in Tables 1 and 2. Twenty-

https://doi.org/10.1346/CCMN.1993.0410105 Published online by Cambridge University Press

Table 1. Calculated X-ray powder diffraction data (CuKα) and angle between {*hkl*} and 001 for <2 μm Cap Rouge 1*M* mica in the range 16° to 40° 2θ.

{*hkl*}	°2θ	d (Å)	I/I$_0$	ξ°
002	17.77	4.992	20	0.0
020	19.77	4.492	70	90.0
110	19.96	4.449	1	80.3
11$\bar{1}$	20.45	4.344	37	74.3
021	21.70	4.096	14	65.8
111	23.22	3.832	<1	58.1
11$\bar{2}$	24.46	3.639	100	53.7
022	26.70	3.339	32	48.0
003	26.79	3.328	43	0.0
112	29.04	3.075	92	42.9
11$\bar{3}$	30.73	2.910	17	40.1
023	33.51	2.674	30	36.5
20$\bar{1}$	34.43	2.605	5	86.3
130	34.70	2.585	23	84.4
13$\bar{1}$	35.00	2.564	47	80.8
200	35.04	2.561	32	78.8
004	35.98	2.496	4	0.0
20$\bar{2}$	36.19	2.482	9	72.0
113	36.33	2.473	2	33.2
131	36.75	2.445	13	70.3
13$\bar{2}$	37.59	2.393	19	67.1
201	37.92	2.372	16	65.4
11$\bar{4}$	38.26	2.352	1	31.4
22$\bar{1}$	40.01	2.253	1	86.8

a = 5.220(8) Å, b = 8.983(10) Å, c = 10.176(18) Å, β = 101.15(0)°. Numbers in parentheses represent the standard deviation in the least significant figure.

ξ = {*hkl*} $\wedge$ 001 ($\leq$90°).

Table 2. Calculated X-ray powder diffraction data (CuKα) and angle between {*hkl*} and 001 for >420 μm Cap Rouge $2M_1$ mica in the range 16° to 40° 2θ.

{*hkl*}	°2θ	d (Å)	I/I$_0$†	ξ°
004	17.76	4.995	27	0.0
020	19.69	4.510	5	90.0
110	19.77	4.492	34	85.1
11$\bar{1}$	19.89	4.465	85	82.0
021	20.19	4.400	10	77.3
111	20.64	4.304	22	72.7
11$\bar{2}$	20.98	4.235	<1	69.9
022	21.62	4.111	20	65.7
112	22.39	3.972	9	61.8
11$\bar{3}$	22.91	3.881	56	59.4
023	23.83	3.735	55	55.9
113	24.84	3.584	3	52.7
11$\bar{4}$	25.51	3.492	79	50.8
024	26.63	3.348	59	47.9
006	26.77	3.330	68	0.0
114	27.82	3.206	80	45.3
11$\bar{5}$	28.60	3.121	7	43.8
025	29.87	2.991	84	41.5
115	31.21	2.866	56	39.5
11$\bar{6}$	32.06	2.792	43	38.3
026	33.45	2.679	<1	36.4
130	34.49	2.600	5	87.2
13$\bar{1}$	34.56	2.595	38	85.4
200	34.64	2.590	19	84.3
116	34.89	2.572	13	34.8
20$\bar{2}$	34.92	2.569	57	80.8
131	35.02	2.563	97	79.8
13$\bar{2}$	35.23	2.548	<1	78.1
11$\bar{7}$	35.80	2.508	9	33.8
008	35.96	2.498	9	0.0
132	36.12	2.487	<1	72.8
13$\bar{3}$	36.46	2.464	25	71.2
202	36.70	2.449	13	70.2
027	37.28	2.412	4	32.3
20$\bar{4}$	37.50	2.400	16	67.1
133	37.75	2.383	39	66.2
13$\bar{4}$	38.21	2.355	<1	64.8
117	38.80	2.321	<1	31.0
11$\bar{8}$	39.76	2.267	1	30.2
134	39.87	2.261	<1	60.3
040	39.98	2.255	1	90.0
22$\bar{1}$	40.01	2.253	10	88.5

a = 5.205(4) Å, b = 9.021(6) Å, c = 20.078(18) Å, β = 95.67(0)°. Numbers in parentheses represent the standard deviation in the least significant figure.

ξ = {*hkl*} $\wedge$ 001 ($\leq$90°).

† I/I$_0$ = 100 for the 002 reflection.

four reflections for 1*M* mica and 42 reflections for $2M_1$ mica have non-zero intensity in the 16° to 40° 2θ range. Both 2θ and *d*-values are given in Tables 1 and 2 for ease in relating *hkl* values with peaks on the diffraction traces shown in the figures that were generated using these data.

Not all *hkl* values shown in Tables 1 and 2 are found in some tabulations given in the literature (e.g., Bailey, 1980). The most notable of these is the 131 of $2M_1$ mica (Table 2), which makes a strong contribution to the intensity of the ~2.58 Å peak, a peak used in quantitative estimates of proportions of 1*M* and $2M_1$ micas. This peak is composed of four unresolved reflections for the 1*M* mica and six unresolved reflections for the $2M_1$ mica; *d*-values of these reflections range from approximately 2.56 to 2.60 Å.

1M mica

Oriented specimen. An XRD pattern of the oriented <2 μm fraction reveals a series of basal orders (Figure 2, top) of a pure mica or illite. This observed pattern is compared with a calculated pattern (Figure 2, bottom; 00*l* only) for the region from 4° to 50° 2θ. A reasonable match is evident, except for the background rise at low angles on the observed pattern; this likely is due to a small number of layers, estimated from 00*l* peak widths as $\leq$20 layers, that is not modeled in the calculated pattern. Additional basal peaks are present

https://doi.org/10.1346/CCMN.1993.0410105 Published online by Cambridge University Press

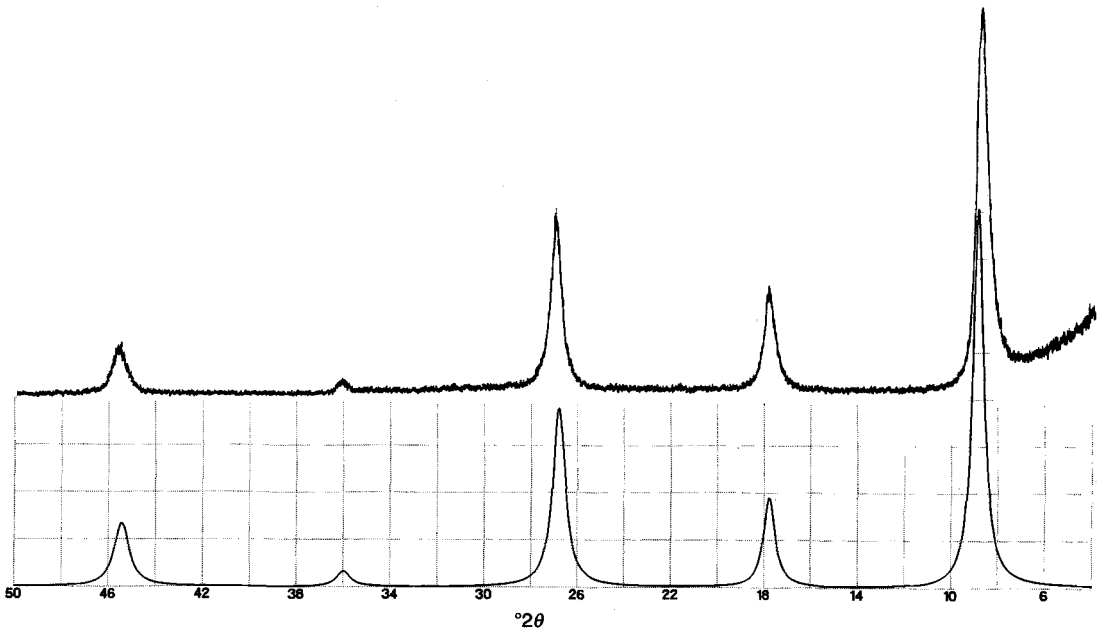

Figure 2. XRD patterns (CuKα) for 1*M* Cap Rouge mica. Top: Observed for <2 μm fraction oriented on glass slide. Bottom: Calculated for 00*l* reflections only.

on the observed pattern at 2θ values >50°. Non-mica peaks are absent.

Observed XRD patterns from this size fraction appear to correspond closely with those presented by Środoń and Eberl (1984) for the Silver Hill (Montana) sample. Changes in peak intensities, peak widths, and *d*-values observed in the XRD patterns of air-dried and glycolated specimens are very similar to those shown in the figure of the Silver Hill sample, except that 001 of the Cap Rouge specimen sharpens upon glycolation. The measured Ir parameter (Środoń, 1984) for this sample is 1.53, and it is estimated to contain not more than ~5% expandable interlayers. These observations show that the <2 μm Cap Rouge mica is similar to micas or illites studied by others.

Unoriented specimen. The XRD pattern (Figure 3, middle) of a relatively unoriented portion of the <2 μm fraction can be indexed as 1*M*. This observed pattern is compared with two calculated patterns in Figure 3. The calculated pattern (top) was formed using the intensities of the 24 reflection planes given in Table 1, each multiplied by an appropriate March function and a scale factor; each March function is dependent on the angle ξ (a function of *hkl*) and a least-squares-determined *r* value of 0.68. The number of peaks and their 2θ values on this calculated pattern are in accord with those on the observed pattern (middle); however, peak heights and peak widths match poorly. Peak widths are variable on the observed pattern, suggesting either the presence of stacking faults parallel to the layers of the mica particles or particles with anisotropic crystallite shapes, i.e., large dimensions parallel to the layers as suggested by the narrow 020 peak and small dimensions perpendicular to the layers as suggested by the wide 002 peak.

The computer program used does not allow for simulation of variable peak widths or stacking faults, but

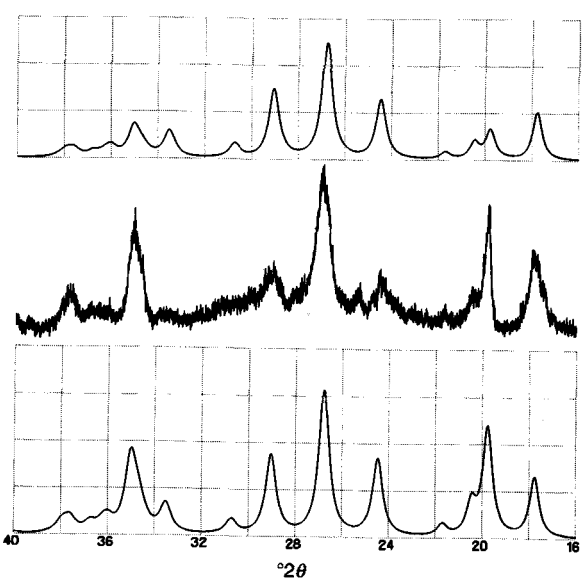

Figure 3. XRD patterns (CuKα) for 1*M* Cap Rouge mica. Top: Calculated with r = 0.68. Middle: Observed for side-packed <2 μm fraction. Bottom: Calculated with r = 0.68 and peak-maximum intensities adjusted for crystallite shape.

https://doi.org/10.1346/CCMN.1993.0410105 Published online by Cambridge University Press

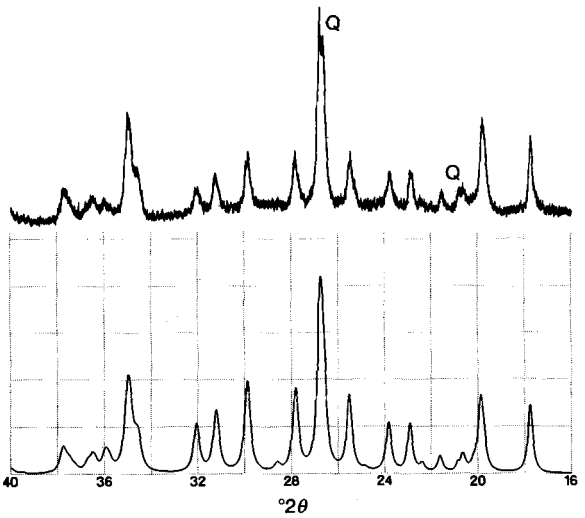

Figure 4. XRD patterns (CuKα) for mixture of $2M_1$ Cap Rouge mica and quartz (Q). Top: Observed for side-packed >420 μm mica flakes. Bottom: Calculated with $r = 0.76$.

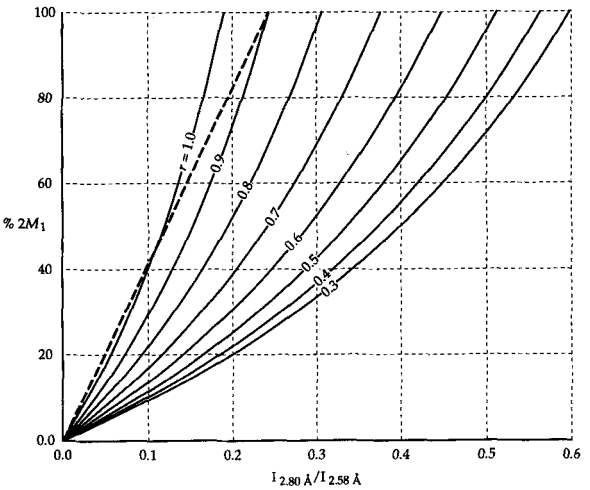

Figure 5. Percentages of $2M_1$ mica in a $1M$–$2M_1$ mixture as a function of the ratio of the intensities (peak areas) of the 2.80 Å and 2.58 Å peaks (CuKα). Solid lines: Calculated for Cap Rouge mica chemical compositions and values of r from $0.3 \leq r \leq 1.0$ in increments of 0.1. Dashed line: Experimental relationship of Maxwell and Hower (1967).

the effect of anisotropic crystallite shapes was treated in the following way: The widths of 002 and 020 were measured at half-maximum intensity on an XRD pattern of a portion of the sample that was heated to 200°C, and the Scherrer equation was employed to calculate mean-crystallite dimensions parallel and perpendicular to the layers, 625 Å and 150 Å, respectively. The mica particles were assumed to be disk shaped, and a mean-crystallite size perpendicular to each *hkl* reflection (Wilson, 1962) was determined. Peak-maximum intensities of all 24 *hkl* reflections (Table 1) were adjusted in proportion to their mean-crystallite size (as opposed to adjusting the peak widths), multiplied by appropriate March functions using an r value of 0.68, and rescaled to match peak heights on the observed pattern. The recalculated pattern is shown in Figure 3 (bottom). Improved agreement with the observed pattern is apparent, but the match is not completely satisfactory. No further attempt was made to improve the agreement because of the ambiguity in the crystal structure of the $1M$ mica.

The peak at 25.5° 2θ on the observed XRD pattern cannot be accounted for with certainty. It is not due to a $1M$ mica whose space group is either C2/m or C2. A peak at this 2θ value is present on XRD patterns of $2M_1$ mica, but no other diagnostic $2M_1$ peaks appear. It is, perhaps, due to anatase.

$2M_1$ mica

Observed (top) and calculated (bottom) patterns for the $2M_1$ mica are shown in Figure 4. The calculated pattern was formed using the intensities of the 42 reflection planes given in Table 2, multiplied by appropriate March functions using a least-squares-determined r value of 0.76 and a scale factor. The number of peaks and their 2θ values, peak intensities, and peak widths on the calculated pattern are generally in accord with those on the observed pattern. Allowance was made on the calculated pattern for the presence of a small amount of quartz. Additional adjustment of the calculated pattern owing to crystallite shape that was necessary for the $1M$ mica was not necessary for the pattern of the $2M_1$ mica.

Quantitative analysis using one peak-area ratio

The experimental relationship of Maxwell and Hower (1967) of % $2M_1$ mica as a function of the 2.80 Å/2.58 Å peak-area ratio is shown in Figure 5. To illustrate the effect of particle orientation on estimates of proportions of $1M$ and $2M_1$ micas, a family of calculated, curved lines is shown that depict the relationship between the two variables when allowance is made for particle orientation using the March function. Use of Maxwell and Hower's relationship appears to give inexact estimates of proportions of $1M$ and $2M_1$ micas, except in samples containing approximately unoriented particles. Although this condition is likely present with synthetic micas whose individual crystals are intergrown with many orientations, such a situation is unlikely with micas that have been dried following dispersal in water and subsequently mounted in flat-surface XRD sample holders. In most instances, use of Maxwell and Hower's relationship in the absence of a correction for preferred orientation gives % $2M_1$ values that are too high and gives more than 100% when the 2.80 Å/2.58 Å peak-area ratio is >0.24.

Intensities of peaks used for estimating proportions

of $1M$ and $2M_1$ micas can vary with different particle orientations. Four $1M$-mica planes—$20\bar{1}$, 130, $13\bar{1}$, and 200 (Table 1)—and six $2M_1$-mica planes—130, $13\bar{1}$, 200, 116, $20\bar{2}$, and 131 (Table 2)—contribute to the intensity of the 2.58 Å peak. (Our calculations agree with Maxwell and Hower's statement that equal amounts of $1M$ and $2M_1$ micas make nearly equal contributions to the intensity of the 2.58 Å peak.) All crystallographic planes of $1M$ and $2M_1$ micas contributing to the 2.58 Å peak, except 116 of $2M_1$, make large angles (ξ) with 001 (Tables 1 and 2). The intensities of these planes decrease with an increase in the preferred orientation, i.e., with a decrease in the value of r. The intensity of 116 of $2M_1$ mica is maximum at $r = 0.62$. Intensities of all $00l$ reflections, such as 002 of $1M$ mica and 004 of $2M_1$ mica ($d = 5.0$ Å), increase with a decrease in r. The intensity of $11\bar{6}$ of $2M_1$ mica ($d = 2.80$ Å), which was used as the numerator by Maxwell and Hower (1967) and in the present study to estimate proportions of $1M$ and $2M_1$ micas, is maximum at $r = 0.68$.

These considerations suggest that quantitative estimates of $1M$ and $2M_1$ micas in mixtures are likely to be inexact in the absence of a correction for preferred orientation.

Quantitative analysis using two peak-area ratios

Peak-area ratio diagram. Numerous patterns were calculated for $1M$–$2M_1$ mixtures for r values from $0.3 \leq r \leq 1.0$ in 0.1 increments and $0 \leq \%\ 2M_1 \leq 100$ in 10% increments. Parameters of the two micas used for these calculations were identical with those that produced the calculated patterns shown in Figures 3 (bottom) and 4 (bottom). The areas under the 5.0 Å, 2.80 Å, and 2.58 Å peaks were integrated by computer and peak-area ratios for 2.80 Å/5.0 Å and 2.80 Å/2.58 Å were formed. A diagram (Figure 6) was constructed from which values of r and % $2M_1$ can be determined as a function of the two peak-area ratios. A second peak-area ratio diagram was calculated in the same way except that the composition $K_{0.8}Al_2(Si_{3.2}Al_{0.8})O_{10}(OH)_2$ was used for the $1M$ mica and the ideal composition of muscovite, i.e., $KAl_2(Si_3Al)O_{10}(OH)_2$, was used for the $2M_1$ mica. The second diagram is also portrayed in Figure 6 and provides a measure of the effect of a change of chemical composition upon the determination of % $2M_1$ mica and particle orientation. The effect of a concomitant change of crystal structure on the peak-area ratio diagram was not considered.

Analysis of intermediate size fractions. From ratios of areas of the specified peaks, measured on observed XRD patterns, Figure 6 yielded r and % $2M_1$ values. *Calculated* patterns were then constructed using mixtures of $1M$ and $2M_1$ micas in the proportions determined from Figure 6 and appropriately modified by the March function using the value of r determined from Figure 6. To model completely the XRD patterns of the Cap Rouge specimens, an appropriate amount of quartz was included in the calculations. Comparisons of representative calculated and observed patterns for three size fractions are shown in Figures 7–9. Estimates of proportions of $1M$ and $2M_1$ micas, r values, percentage of quartz, and method of sample mounting are given in Table 3 for all size fractions used in this study. Percentages of quartz and both micas used for drawing the calculated patterns are given without parentheses in this table; numbers in parentheses for the micas represent proportions determined from the peak-area ratio diagram (Figure 6).

Agreement between the calculated and observed XRD patterns for the intermediate size fractions appears to be reasonable and comparable to that shown by the pure micas although the matches are not exact. The least oriented specimens, i.e., those with values of r closest to unity, are shown by side-packed samples (Figures 3 and 4); the most oriented specimen is the front-packed sample (Figure 7). The results are in accord with expectations for these sample mounts.

The peak-area ratio diagram (Figure 6) may be used by other investigators to determine proportions of $1M$ and $2M_1$ micas in their samples. Subsequent calculation of patterns as was done here is not necessary. Quantities determined from the peak-area ratio diagram are likely to be more accurate than those determined from Maxwell and Hower's diagram because of the inclusion of the effect of particle orientation in the present study. However, Maxwell and Hower's method and the present method are applicable strictly to the micas used in the two studies. The extent of possible error in quantitative estimates of micas having different chemical compositions and crystal structures by using either of these methods is moot.

A further test of the utility of the diagram to estimate mica proportions in mixtures would be to physically mix pure $1M$ and $2M_1$ micas in various proportions and analyze the XRD patterns using the described procedures. We have not undertaken this experiment.

Consideration of possible sources of error

Several assumptions were made in the calculation of patterns which may affect the obtained results. These include the following:

1) The muscovite crystal structure of Rothbauer (1971) applies to the $2M_1$ Cap Rouge mica even though the chemical compositions are not identical.

2) A transformation of the muscovite crystal structure of Rothbauer (1971) to space group $C2/m$ approximates the $1M$ Cap Rouge mica structure.

3) Scattering factors for neutral atoms are more appropriate for calculating patterns than are ionic scattering factors.

https://doi.org/10.1346/CCMN.1993.0410105 Published online by Cambridge University Press

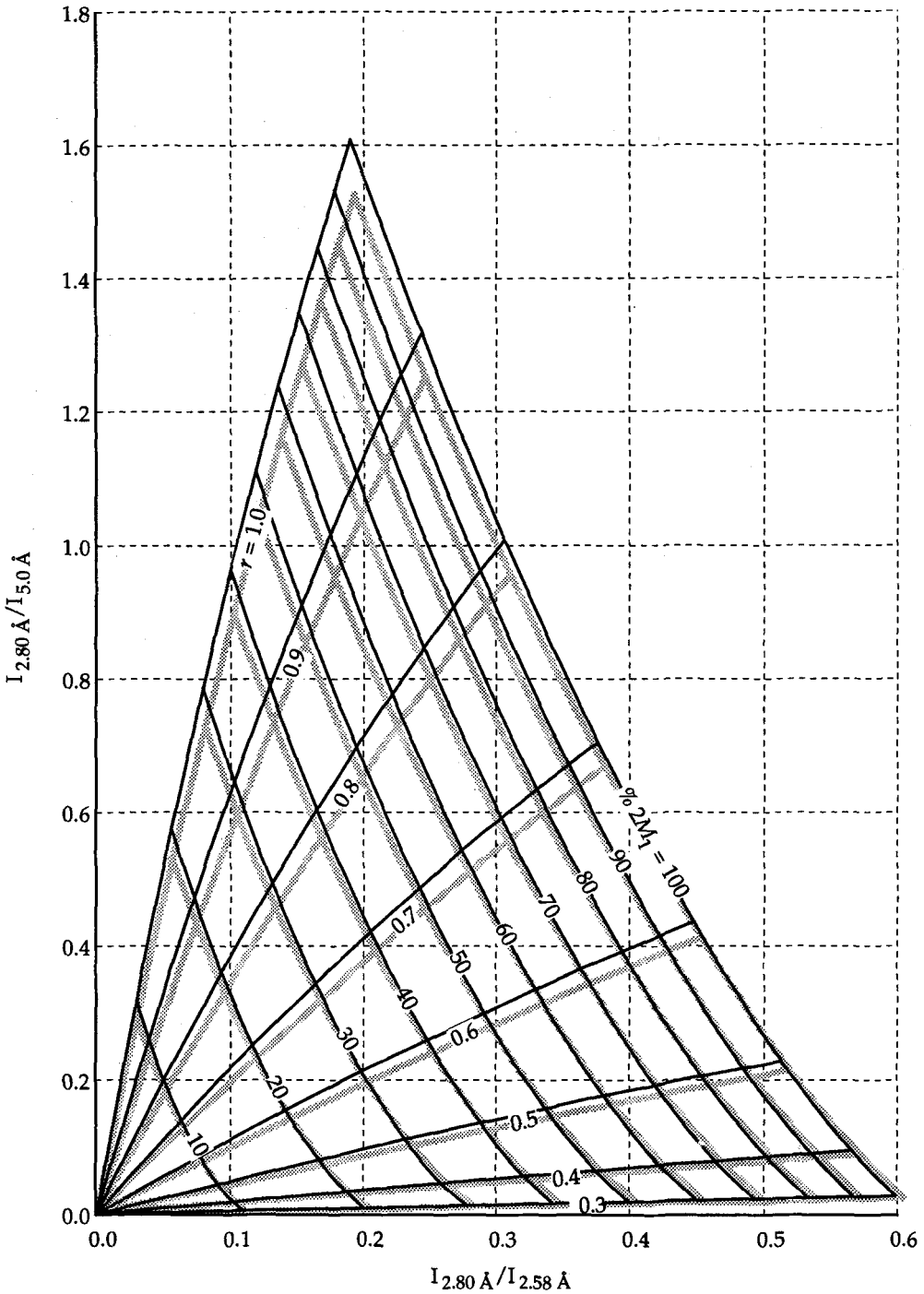

Figure 6. Percentages of $2M_1$ mica in a $1M$–$2M_1$ mixture and values of r as a function of the ratios of the intensities (peak areas) for the 2.80 Å and 5.0 Å peaks and the 2.80 Å and 2.58 Å peaks (CuKα). Solid lines: Calculated for Cap Rouge mica chemistries. Stippled lines: Calculated for $K_{0.8}Al_2(Si_{3.2}Al_{0.8})O_{10}(OH)_2$ composition for $1M$ mica and $KAl_2(Si_3Al)O_{10}(OH)_2$ composition for $2M_1$ mica.

4) Crystal structure and chemical composition of each mica are not a function of particle size.

The effects that some alternative assumptions had on the calculated patterns were examined, but no rigorous comparisons were made.

Sample preparation and the March function

It might appear that the March function has been misapplied to our side-packed specimens. The March function as described by Dollase (1986) for powder

https://doi.org/10.1346/CCMN.1993.0410105 Published online by Cambridge University Press

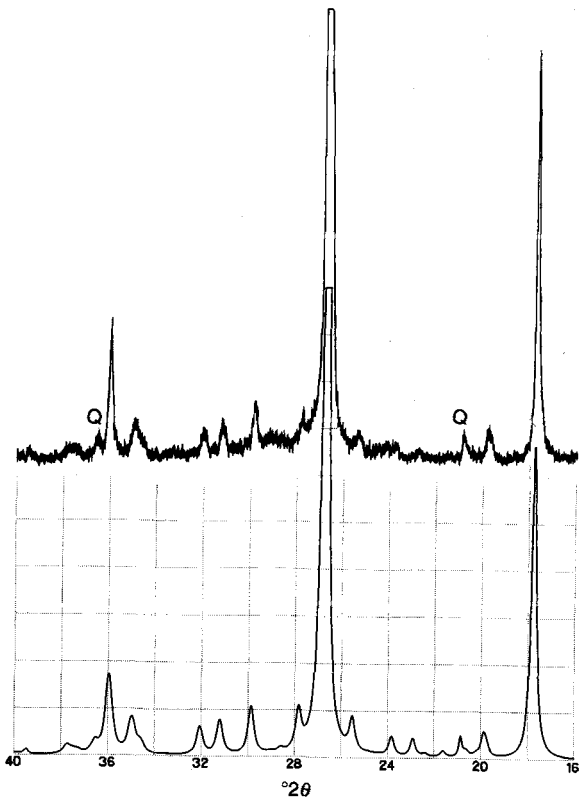

Figure 7. XRD patterns (CuKα) for mixtures of Cap Rouge micas and quartz (Q). Top: Observed for front-packed >105 μm fraction. Bottom: Calculated with $r = 0.42$. The value of r was determined using Figure 6 and peak-area ratios of the observed pattern.

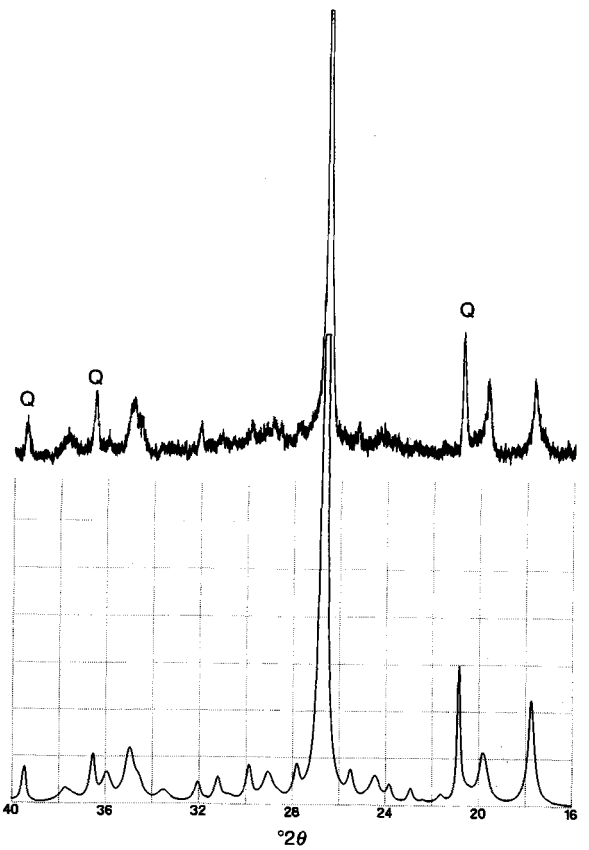

Figure 8. XRD patterns (CuKα) for mixtures of Cap Rouge micas and quartz (Q). Top: Observed for back-packed 53–105 μm fraction. Bottom: Calculated with $r = 0.57$. The value of r was determined using Figure 6 and peak-area ratios of the observed pattern.

Table 3. Estimates of weight percentages of components in various size fractions of the Cap Rouge sample compared with percentages determined with the relationship of Maxwell and Hower (1967).

Size fraction (μm)	% 1M	% 2M_1	% Qtz	r	Remarks	Figure # of XRD pattern	% 2M_1 (M&H)
>420*	0	99	1	0.76	r value from least sqs.; s.p.	4	94
>105*	9 (14)†	85 (86)	6	0.42	r value from p.a.r.d.; f.p.	7	>100
53–105	58 (72)	22 (28)	20	0.57	r value from p.a.r.d.; b.p.	8	73
20–53	65 (86)	10 (14)	25	0.63	r value from p.a.r.d.; b.p.	—	40
10–20	88 (92)	8 (8)	4	0.59	r value from p.a.r.d.; b.p.	9	25
5–10	93	7	tr.	0.54	r value from p.a.r.d.; b.p.	—	25
2–5	100	0	0	n.d.	approx. same pattern as <2 μm	—	0
<2	100	0	0	0.68	r value from least sqs.; s.p.	3	0

* Majority of quartz separated from sample prior to recording XRD pattern.
† Percentages in parentheses are from the peak-area ratio diagram (p.a.r.d., Figure 6) and do not include quartz.
Qtz = quartz; r = March parameter; M&H = Maxwell and Hower (1967); tr. = trace; n.d. = not determined; s.p. = side-packed; f.p. = front-packed; b.p. = back-packed.

https://doi.org/10.1346/CCMN.1993.0410105 Published online by Cambridge University Press

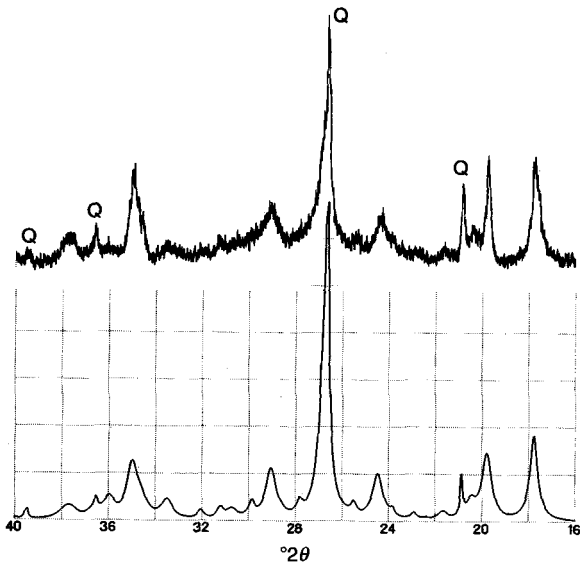

Figure 9. XRD patterns (CuKα) for mixtures of Cap Rouge micas and quartz (Q). Top: Observed for back-packed 10–20 μm fraction. Bottom: Calculated with $r = 0.59$. The value of r was determined using Figure 6 and peak-area ratios of the observed pattern.

diffraction assumes that the particles are effectively rod- or disk-shaped and that, collectively, particles in the sample exhibit cylindrical symmetry with an axis perpendicular to the surface upon which X-rays are incident. Microscopic examination of the Cap Rouge mica particles confirms their flake (or disk) shape, thus satisfying the first assumption. We expect that front- or back-packing would impart cylindrical symmetry about an axis perpendicular to the exposed specimen surface, thus satisfying the second assumption. It might be expected that side-packing would result in a symmetry axis parallel to the exposed specimen surface, thereby invalidating the second assumption. However, our results show no relative decrease in peak heights for 00*l* reflections. Apparently side-packing of mica particles results in a significant orientation parallel to and at the bounding surface (e.g., a glass plate which temporarily constrains the surface to be presented to X-rays).

Values of the March parameter (r) obtained in this study ranged from 0.76 for a side-packed specimen to 0.42 for a front-packed specimen, which agrees with the generally accepted expectation that side-packing produces the least amount of preferred orientation. Further confirmation that the March function appears to be applicable to the three types of specimen packing is the reasonably good agreement between all the calculated and observed XRD patterns.

CONCLUSIONS

Calculated patterns approximate observed XRD patterns of pure Cap Rouge micas when allowance is made for particle orientation by means of the March function despite uncertainties in crystal-structure parameters. Values for the March parameter r and % $2M_1$ are obtained from a computed peak-area ratio diagram for *mica mixtures* from which patterns were calculated; these patterns also compare reasonably well with observed XRD patterns. Quantitative estimates obtained using the peak-area ratio diagram are believed to be more exact than those obtained using previously described methods. The diagram, without further calculation of patterns, may be of general use for estimating proportions of $1M$ and $2M_1$ micas in mixtures of the two, even in the presence of impurities. It is hoped that this investigation may stimulate additional studies concerned with quantitative estimates of mica mixtures. An obstacle to improved quantitative estimates with any procedure involving XRD is the lack of accurate crystal-structure data for $1M$ mica.

REFERENCES

Bailey, S. W. (1980) Structures of layer silicates: in *Crystal Structures of Clay Minerals and Their X-ray Identification,* G. W. Brindley and G. Brown, eds., Mineralogical Society, Monogr. **5,** London.

Bailey, S. W. (1988) X-ray diffraction identification of the polytypes of mica, serpentine, and chlorite: *Clays & Clay Minerals* **36,** 193–213.

Bargar, J. (1990) *Crystal chemistry of a $2M_1$ muscovite:* Senior thesis, Department of Geology and Mineralogy, The Ohio State University, Columbus, Ohio.

Corbató, C. E. and Tettenhorst, R. T. (1982) Two examples of quantitative analysis by simulated X-ray powder diffraction patterns: *Clay Miner.* **17,** 393–399.

DiMarco, M. J., Ferrell Jr., R. E., and Lowe, D. R. (1989) Polytypes of 2:1 dioctahedral micas in silicified volcaniclastic sandstones, Warrawoona Group, Pilbara Block, Western Australia: *Amer. J. Sci.* **289,** 649–660.

Dollase, W. A. (1986) Correction of intensities for preferred orientation in powder diffractometry: Application of the March model: *J. Appl. Crystallogr.* **19,** 267–272.

Eberl, D. D., Środoń, J., Lee, M., Nadeau, P. H., and Northrop, H. R. (1987) Sericite from the Silverton Caldera, Colorado: Correlation among structure, composition, origin, and particle thickness: *Amer. Mineral.* **72,** 914–934.

Foord, E. E., Martin, R. F., Fitzpatrick, J. J., Taggart Jr., J. E., and Crock, J. G. (1991) Boromuscovite, a new member of the mica group, from the Little Three mine pegmatite, Ramona district, San Diego County, California: *Amer. Mineral.* **76,** 1998–2002.

Foscolos, A. E. and Kodama, H. (1974) Diagenesis of clay minerals from lower Cretaceous shales of north eastern British Columbia: *Clays & Clay Minerals* **22,** 319–335.

Inoue, A., Kohyama, N., Kitagawa, R., and Watanabe, T. (1987) Chemical and morphological evidence for the conversion of smectite to illite: *Clays & Clay Minerals* **35,** 111–120.

Kisch, H. J. (1983) Mineralogy and petrology of burial diagenesis (burial metamorphism) and incipient metamorphism in clastic rocks: in *Diagenesis in Sediments and Sedimentary Rocks,* 2nd ed., G. Larsen and G. V. Chilingar, eds., Developments in Sedimentology **25B,** Elsevier, Amsterdam, 289–493.

March, A. (1932) Mathematische Theorie der Regelung nach der Korngestalt bei affiner Deformation: *Z. Kristalogr.* **81,** 285–297.

Maxwell, D. T. and Hower, J. (1967) High-grade diagenesis and low-grade metamorphism of illite in the Precambrian Belt Series: *Amer. Mineral.* **52,** 843–857.

Meunier, A. and Velde, B. (1989) Solid solutions in I/S mixed-layer minerals and illite: *Amer. Mineral.* **74,** 1106–1112.

Post, J. E. and Bish, D. L. (1989) Rietveld refinement of crystal structures using powder X-ray diffraction data: in *Modern Powder Diffraction,* D. L. Bish and J. E. Post, eds., MSA Reviews in Mineralogy **20,** 277–308.

Reynolds Jr., R. C. (1963) Potassium-rubidium ratios and polymorphism in illites and microclines from the clay size fractions of Proterozoic carbonate rocks: *Geochim. Cosmochim. Acta* **27,** 1097–1112.

Rothbauer, R. (1971) Untersuchung eines $2M_1$-Muskovits mit Neutronenstrahlen: *Neues Jahrb. Mineral. Monatsh.* **4,** 143–154.

Sidorenko, O. V., Zvyagin, B. B., and Soboleva, S. V. (1975) Crystal structure refinement for 1M dioctahedral mica: *Soviet Phys. Crystallogr.* **20,** 332–335.

Środoń, J. (1984) X-ray powder diffraction identification of illitic materials: *Clays & Clay Minerals* **32,** 337–349.

Środoń, J. and Eberl, D. D. (1984) Illite: in *Micas,* S. W. Bailey, ed., MSA Reviews in Mineralogy **13,** 495–544.

Velde, B. (1965) Experimental determination of muscovite polymorph stabilities: *Amer. Mineral.* **50,** 436–449.

Velde, B. and Hower, J. (1963) Petrological significance of illite polymorphism in Paleozoic sedimentary rocks: *Amer. Mineral.* **48,** 1239–1254.

Weaver, C. E. and Broekstra, B. R. (1984) Illite-mica: in *Shale-Slate Metamorphism in Southern Appalachians,* C. E. Weaver, ed., Developments in Petrology **10,** Elsevier, Amsterdam, 67–97.

Wilson, A. J. C. (1962) *X-ray Optics:* 2nd ed., Methuen & Co. Ltd., London.

Yoder, H. S. and Eugster, H. P. (1955) Synthetic and natural muscovites: *Geochim. Cosmochim. Acta* **8,** 225–280.

(Received 25 August 1992; accepted 19 January 1993; Ms. 2270)